Exploring the impact of hydrostatic pressure on the structural, electronic and mechanical properties of ZrNiPb half-Heusler alloy: A DFT approach

Article *in* International Journal of Modern Physics B · July 2018

DOI: 10.1142/S021797921850248X

Michael Babalola
University of Benin

Bamidele ibrahim Adetunji
Bells University of Technology

Ben Erhunmwunse Iyorzor
University of Benin

Abu Yaya
University of Ghana

International Journal of Modern Physics B
Vol. 32 (2018) 1850248 (12 pages)

DOI: 10.1142/S021797921850248X

Exploring the impact of hydrostatic pressure on the structural, electronic and mechanical properties of ZrNiPb half-Heusler alloy: A DFT approach

M. I. Babalola*, B. I. Adetunji[†,§], B. E. Iyorzor* and A. Yaya[‡]

*Department of Physics,
University of Benin, Benin City, Nigeria

[†]Department of Physical Sciences,
Bells University of Technology, Ota, Nigeria

[‡]Department of Materials Science and Engineering,
University of Ghana, Accra, Ghana

[§]adetunji@physics.unaab.edu.ng

Received 19 February 2018
Revised 5 June 2018
Accepted 6 June 2018
Published 27 July 2018

The structural, electronic, elastic and mechanical properties of ZrNiPb half-Heusler alloy under pressure ranging from 0 to 25 GPa have been studied using the density functional theory within the generalized gradient approximation (GGA). The results of ambient condition were in good agreement with the available theoretical and experimental data. Our electronic structure and density of state results show that ZrNiPb is an indirect bandgap semiconductor half-Heusler alloy with a narrow energy gap of 0.375 eV. Based on the calculated elastic constants (C_{11}, C_{12} and C_{44}), Young's modulus (E), Poisson's ratio (ν), Shear modulus (G), Zener anisotropy factor (A) and brittle-ductile behaviors under pressure have been discussed. The calculated Poisson's ratio shows that ZrNiPb undergoes a relatively small volume change during uniaxial deformation. We show that the chemical bonds in ZrNiPb are stronger due to the high value of C_{11}.

Keywords: First principles; structural properties; electronic properties; mechanical properties.

PACS numbers: 31.10.+z, 31.15.E+, 63.20.Dj, 65.40.−b

1. Introduction

For more than a decade, half-Heusler alloys have attracted a lot of interest from the scientific community because they are among the most promising thermoelectric materials, spintronics materials, transparent conductors and topological

[§]Corresponding author.

semimetals.[1–3] Many of these half-Heusler alloys have been reported with narrow bandgap, high thermopower, high electrical conductivity, large power factor at room-temperature.[4–6] Among these alloys is ZrNiPb which was recently synthesized[7] as an indirect bandgap semiconductor half-Heusler compound with thermopower and power factor of $-153.9\ \mu$V/K and 5.2 μWcm^{-2}K^{-1} at room-temperature. Also, a recent first-principles calculation was performed on series of Pb-based half-Heusler alloys with inclusion of ZrNiPb with suggestions that tuning the doping levels and composition can improve their thermoelectric performance.[8] However, the in-depth knowledge of thermoelectric properties of half-Heusler alloys should not be the only requirement for their industrial applications without the knowledge of their mechanical properties.[9] The mechanical properties are essential for modeling the stress and strain behavior of thermoelectric module within a temperature gradient under the influence of external forces. Even though these properties were essential, only limited information from experiments[10,11] and theory[9,12,13] are available in the literature on mechanical properties of half-Heusler alloys. Meanwhile, the structural, electronic, thermoelectric and elastic properties of ZrNiPb had been examined at zero pressure in a recent work,[14] and it was established that ZrNiPb is mechanically and thermodynamically stable at ambient condition.[14] However, to the best of our knowledge, the structural, electronic and mechanical properties of ZrNiPb have not been examined under applied pressure. Likewise, the effect of pressure on the energy gap around the Fermi level and the bonding characteristics of ZrNiPb are still unknown. Pressure as one of the intensive properties, plays an important role on the structural and electronic properties of materials.[15] Therefore, the objective of this work is to investigate the pressure-induced behavior of the structural, electronic and mechanical properties of ZrNiPb under applied pressure ranging from 0 to 25 GPa using first-principles calculation with projector-augmented wave and plane-wave pseudo-potential density functional theory method.

2. Computational Methods

In this work, calculations were performed using the plane-wave pseudopotential method and the projected augmented wave (PAW) within the generalized gradient approximation GGA[16] using the QUANTUM ESPRESSO code.[17] The PAW dataset (`Zr.pbe-spn-kjpaw_psl.0.2.3.UPF`, `Ni.pbe-n-kjpaw_psl.0.1.UPF` and `Pb.pbe-dn-kjpaw_psl.0.2.2.UPF`) used was taken from the PS library project.[18] The crystal structure of half-Heusler ZrNiPb alloy considered in this work crystallized in a noncentrosymmetric structure with a space group F$\bar{4}$3m and the unit cell consists of interpenetrating face-centered cubic (FCC) sublattices with position Zr (0,0,0), Ni ($\frac{1}{4}$,$\frac{1}{4}$,$\frac{1}{4}$) and Pb ($\frac{3}{4}$,$\frac{3}{4}$,$\frac{3}{4}$). We have used 12-atom unit cell for ZrNiPb at six different pressure states between 0 and 25 GPa. A complete structural relaxation was performed at each pressure state using Broyden, Fletcher, Goldfarb and Shannon (BFGS) approach[19] to correctly determine the energetically stable lattice constant and relaxed atomic positions. In order to achieve convergence of our results, a plane wave basis set with a kinetic energy cut-off of 70 Ry was applied and for the brillouin zone sampling, a $8 \times 8 \times 8$ Monkhorst-Pack meshes[20] was used for all the pressure values considered for ZrNiPb in this work.

The elastic constants were obtained after performing energy-strain calculations with the applications of little strain to an optimized unit cell. Also, the Broyden, Fletcher, Goldfarb and Shannon (BFGS)[19] quasi-newton algorithm was used to perform the relaxation of the atomic positions under the applied strain at each pressure state. The energy of a solid under strain is given as[21,22]

$$\delta E = E_{\mathrm{tot}} - E_0 = \frac{V}{2}\sum_{i=0}^{6}\sum_{j=0}^{6} C_{ij} e_i e_j, \tag{1}$$

where V is the volume of the unstrained lattice cell, δE is the change in energy when strain is applied on the lattice cell, while e_i and e_j are the strain vectors and C_{ij} is the elastic constant matrix. There are three independent elastic constants in a cubic system, they are C_{11}, C_{12} and C_{44}. In other to compute these parameters, we have applied a tri-axial shear strain and volume-conserving orthorhombic strain to strain the lattice cell.[23] These two strains allow us to calculate the C_{44} and shear modulus $G = \frac{1}{2}(C_{11} - C_{12})$. Other elastic stiffness such as Poisson's ratio (ν), Young's modulus (E) and Zener anisotropy factor (A) are obtained from these parameters using the set of equations in Ref. 23.

3. Results and Discussion

3.1. *Structural properties*

We performed series of self-consistent calculations so as to optimize the structure of ZrNiPb. The data sets generated from the self-consistent total energy calculations were fitted to the third-order Birch–Murnaghan equation of state[24] and the equilibrium lattice constant (a_o), bulk modulus (B) and pressure derivative (B') were obtained and presented in Table 1 at zero pressure along with other theoretical and experimental data. The bulk modulus measures how resistant a material is to compressibility and its pressure derivative measures its response to slight increase in pressure. From our calculated value, we observed that ZrNiPb will be easily compressed due to the small value of its bulk modulus. Our calculated lattice constant

Table 1. Calculated lattice constant (a), bulk modulus (B) and pressure derivative (B') of ZrNiPb half-heusler alloy at ambient condition.

Compound	Ref.	a (Å)	B (GPa)	B' (GPa)
ZrNiPb	Present	6.247	110.900	4.710
	Cal. (Ref. 14)	6.232	112.500	—
	Cal. (Ref. 25)	6.270	—	—
	Exp. (Ref. 7)	6.267	—	—

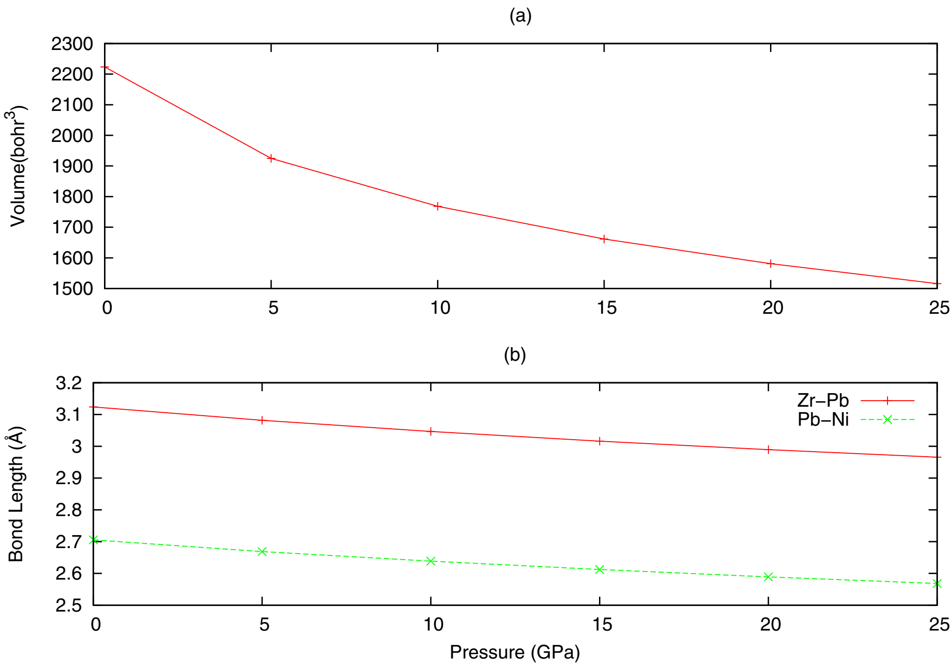

Fig. 1. (Color online) Variation of volume and bond length of ZrNiPb half-Heusler alloy as a function of pressure.

is in good agreement with theoretical values reported in Refs. 14, 25 and experimental value in Ref. 7. However, from our calculated value, there is about 0.32% deviation from the available experimental value in Ref. 7.

Figure 1(a) shows the relationship between the volume and pressure for ZrNiPb between 0 and 25 GPa with the step of 5 GPa. In order to obtain this, the equilibrium geometries of ZrNiPb unit cells were calculated through a complete optimization of the structural parameters at each pressure state. We observed from the graph that as the pressure increases, the volume decreases in a nonlinear relationship. This phenomenon could lead to an increase in covalent bonding and decrease in inter-atomic distances. Our calculated equilibrium Zr–Pb and Pb–Ni inter-atomic distances are 3.124 and 2.705 Å, respectively. The Zr–Pb inter-atomic distances are larger than Pb–Ni inter-atomic distances by 15.47% at ambient condition. At present, there are no experimental and theoretical values to compare with our data. Figure 1(b) shows the response of inter-atomic distances in ZrNiPb to pressure. The Pb–Ni and Zr–Pb bond lengths decrease monotonously with pressure. This behavior could lead to stronger atomic interactions. From Figs. 1(a) and 1(b), we can conclude that Pb–Ni bond is more sensitive to pressure than Zr–Pb bond and the degree of covalence in ZrNiPb is bond length-dependent. These are due to the fact that under applied pressure, the bond length decreases, and more covalent components become available.

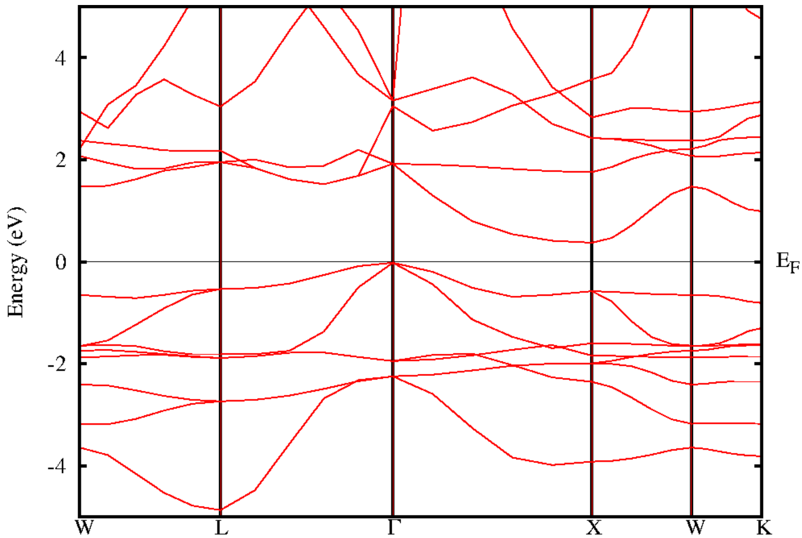

Fig. 2. (Color online) The band structure of ZrNiPb along high-symmetry points.

3.2. *Electronic properties*

The electronic band structure of ZrNiPb in the primitive unit cells at zero pressure along the high-symmetry direction of the Brillouin zone is presented in Fig. 2. From the figure, with the primitive unit cell with high-symmetry points $W \rightarrow L \rightarrow \Gamma \rightarrow X \rightarrow W \rightarrow K$, we observed that the conduction band minimum (CBM) centered at X point and the valence band maximum (VBM) centered at Γ indicates that ZrNiPb is an indirect bandgap semiconductor with a narrow bandgap of 0.375 eV. This indirect bandgap observation is similar to what was observed for ZrNiSn and HfNiSn.[26] Our calculated bandgap of 0.375 eV is in close agreement with the theoretical value of 0.37 eV reported in Ref. 25, 0.40 eV[8] and 0.43 eV reported in Ref. 7. The present result confirmed the previously reported findings in Refs. 7, 14 that ZrNiPb is an indirect bandgap semiconductor material. In Figs. 3 and 4, we presented the band structures of conventional unit cells of ZrNiPb with 12-atoms under pressure along the high-symmetry points $\Gamma \rightarrow X \rightarrow M \rightarrow \Gamma \rightarrow R$. Under the applied pressure, the bandgap decreases monotonously as shown in Fig. 5. However, within the pressure range considered in this work, ZrNiPb retained its semiconductor property. We conclude that there is no possibility for semiconductor-metal transition between 0 and 30 GPa in ZrNiPb half-Heusler alloy.

For a better understanding of the bonding characteristic and to exploit the underlying structural stability and elastic properties, we calculated and presented in Fig. 6, the density of states (DOS) and the projected density of states (PDOS) for ZrNiPb showing the total density of states (TDOS) and the contributions of the Zr, Ni and Pb orbitals to the density of states at ambient pressure. This also confirmed that ZrNiPb is a semiconductor with a narrow gap between the occupied

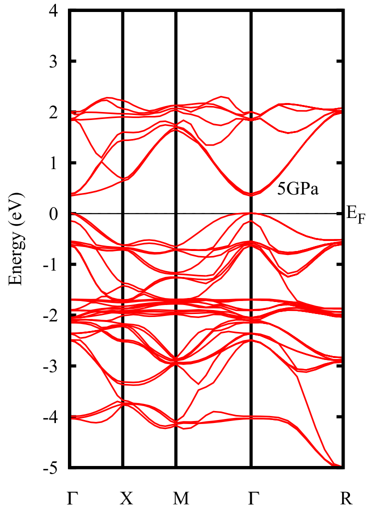

Fig. 3. (Color online) The band structure of ZrNiPb along high-symmetry points at 5 and 10 GPa.

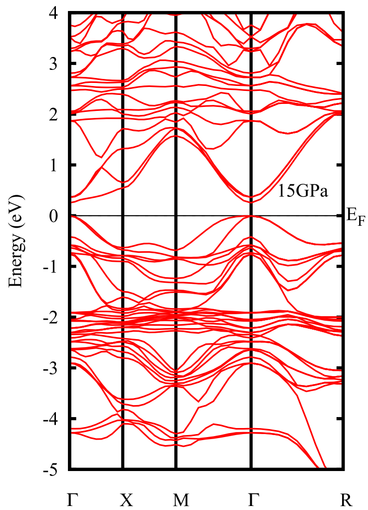

Fig. 4. (Color online) The band structure of ZrNiPb along high-symmetry points at 15 and 20 GPa.

and unoccupied regions around the Fermi level. In the occupied region between 0 and −4.0 eV, there are five pronounced peaks which are the contributions from the valence electron of Ni-2p/3d, Pb-2p/3d and Zr-4p/5d orbitals. However, the contributions from Ni-2p, Pb-3d and Zr-4p orbitals are smaller in magnitude as shown in Fig. 6. Near the Fermi level, the TDOS of ZrNiPb is dominated by Zr-5d orbital and little contributions from Pb-2p and Ni-2p/3d orbitals. In the occupied region, Ni-3d and Zr-5d are the major orbitals that dominate the TDOS around

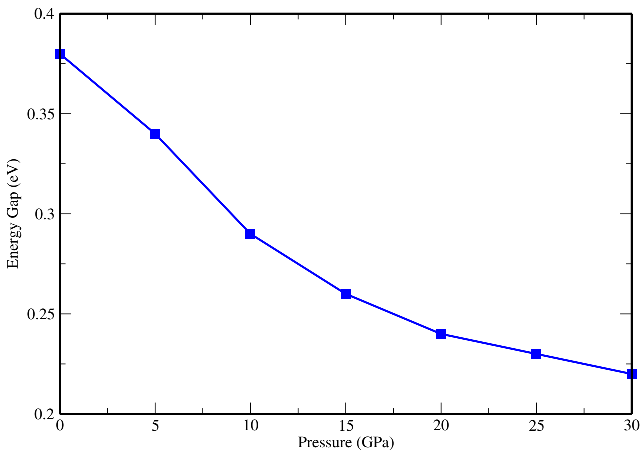

Fig. 5. (Color online) The variation of the energy gap (eV) of ZrNiPb half-Heusler alloy as a function of pressure.

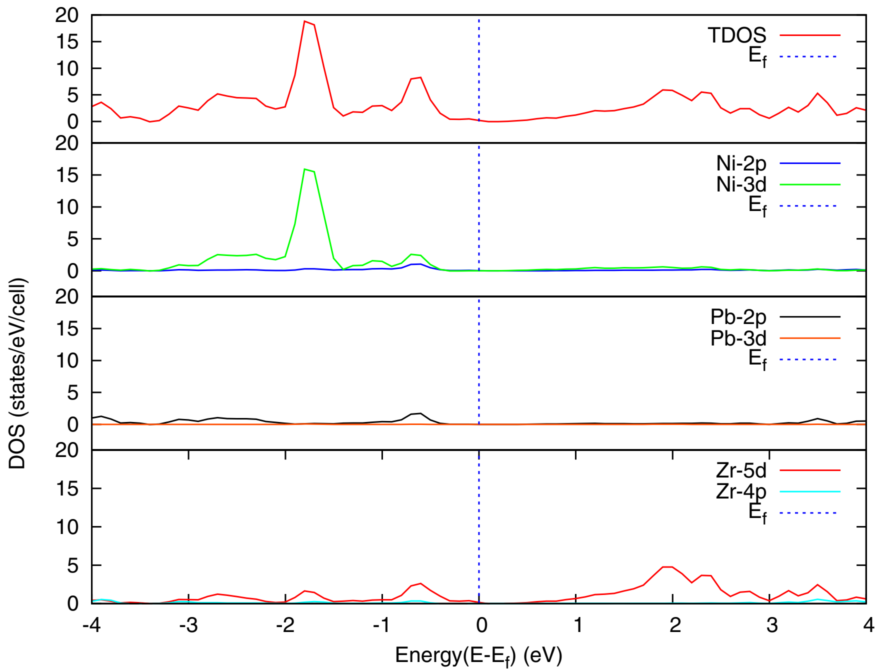

Fig. 6. (Color online) Total and PDOSs of ZrNiPb at zero pressure.

−1.85 eV. Between −0.4 and −1.0 eV, Zr-5d, Ni-3d and Pb-2p contribute largely to the TDOS. Above the Fermi level, between 0 and 4.0 eV, we observed a clear dominant of Zr-5d orbitals. In the TDOS plot, there is a pseudogap near the Fermi level which is due to a strong covalent interaction between 2p states of Ni/Pb, 3d

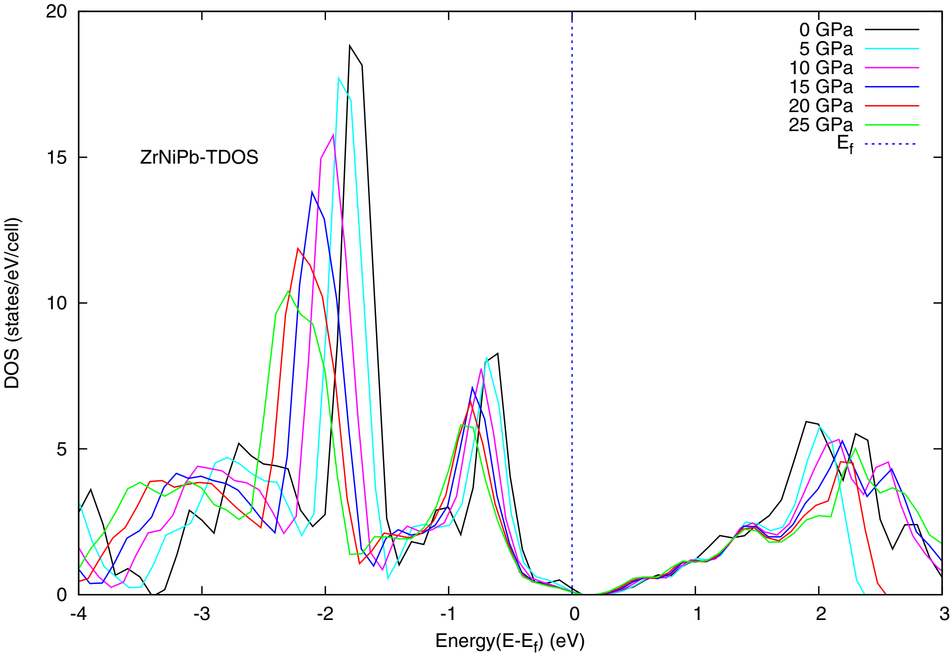

Fig. 7. (Color online) Total DOS of ZrNiPb under different pressures.

state of Pb, 4p/5d states of Zr. This is an indication that a strong hybridization effect exits in ZrNiPb half-Heusler alloy at zero pressure. This observation could lead to bonding and anti-bonding orbital separation[27] and could contribute to the stability of ZrNiPb. Therefore, the interaction between Zr-5d, Ni-3d and Pb-2p orbitals contribute to the structural stability of ZrNiPb half-Heusler alloy.

We have investigated the response of the DOS and TDOS of ZrNiPb to applied pressure, the TDOS are presented in Fig. 7. As the pressure increases, the shapes of the peaks changes slightly. This is an indication that ZrNiPb is structurally stable and there is no possibility of phase transformation in the pressure range considered in this work. Looking at Fig. 7, there are significant offsets in the TDOSs as the pressure increases. These offsets are the results of change of interaction potentials which lead to the reduction in the distance between the atoms under pressure.[28] Therefore, the peaks in the unoccupied regions (anti-bonding regions) moved toward the higher energy regions and the peaks in the occupied regions (bonding regions) moved away to the left under the applied pressure. Furthermore, we noticed that all the peak heights reduced as the pressure increased and there was reduction in the hybridization energy as the pressure increased. Also, the peaks in the unoccupied regions became weaker as the pressure increased. This implies that the hybridization between Zr-5d orbital and other orbitals is weaker under pressure. Based on our observations, we conclude that ZrNiPb will undergo semiconductor-metal transition at higher pressure than the range considered in this work.

3.3. *Elastic properties*

The link between the mechanical and the dynamical behaviors of crystalline materials depends on the elastic constants of solids which provide an important information concerning the nature of the forces operating in solid materials. The behavior of crystalline materials to an external applied stress depends on bulk modulus, shear modulus, Young's modulus, Piosson's ratio and anisotropy.[29] They play essential roles in understanding their structural stability and anisotropic characteristics. We calculated the elastic constants by straining ZrNiPb crystal structure with seven points of strain between -0.03 and 0.03 in steps 0.01 for the tri-axial shear strain and volume-conserving orthorhombic strain, respectively. The values of the elastic constants (C_{11}, C_{12} and C_{44}), Young's modulus (E), Poisson's ratio (ν), Shear modulus (G) and Zener anisotropy factor (A) calculated at zero pressure are presented in Table 2. As shown in Table 2, our calculated elastic constants (C_{11}, C_{12} and C_{44}) are in good agreement with the recently reported theoretical values in Ref. 14 and presently there are no experimental data to compare with our results. Our calculated Poisson's ratio of 0.23 shows that ZrNiPb undergoes a relatively small volume change during uniaxial deformation. The higher value of C_{11} is an indication that the chemical bonds in ZrNiPb are stronger.

The shear elastic deformation which depends on the ratio (G/B) is a parameter that could be used to detect a favorable thermoelectric materials,[30] the smaller the value, the favorable the materials are for thermoelectric application. Our calculated value of G/B of 0.6636 shows that ZrNiPb has low resistance opposed to shear deformation and good machinability because it is less than the value (1.06) for the reference fragile material α-SiO_2.[31] Furthermore, our calculated elastic constants (C_{11}, C_{12} and C_{44}) for ZrNiPb satisfied the following mechanical stability conditions for cubic structure: $C_{11} - C_{12} > 0$, $C_{44} > 0$ and $C_{11} + 2C_{12} > 0$. The smaller value of C_{12} is an indication that ZrNiPb is elastically stable.

The empirical relationship between bulk and Young's moduli (B/G) as proposed by Pugh[32] could be used to describe the mechanical strength of materials. He suggested that if the B/G ratio is less than 1.75, the material is brittle in nature and otherwise, it is ductile. Relaying on this assumptions, we found that the B/G ratio for ZrNiPb is 1.51. This implies that ZrNiPb is brittle in nature at ambient condition. Further analysis using the Poisson's ratio shows that materials with values greater than 0.33 are ductile and those with values lesser than 0.33 are brittle,[33] hence the calculated value of 0.23 also confirmed that ZrNiPb is brittle in nature.

Table 2. Calculated elastic constants (C_{11}, C_{12} and C_{44}), Young's modulus (E), Poisson's ratio (ν), Shear modulus (G) and Zener anisotropy factor (A) in (GPa) for ZrNiPb half-Heusler alloy at ambient condition.

Compound	Ref.	C_{11}	C_{12}	C_{44}	G	E	G/B	ν	A
ZrNiPb	Present	209.02	61.84	55.94	73.59	180.78	0.664	0.23	0.76
	Cal. (Ref. 14)	205.50	66.00	58.80	72.80	179.60	0.647	—	—

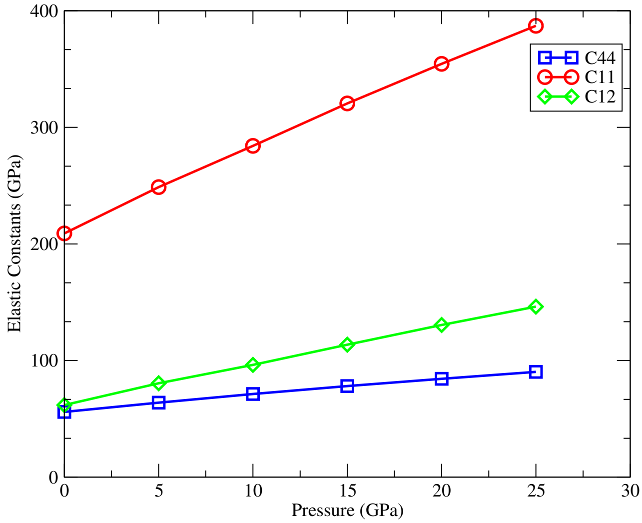

Fig. 8. (Color online) Calculated pressure dependence of elastic constants (C_{11}, C_{12} and C_{44}) for ZrNiPb half-Heusler alloy.

In Fig. 8, we presented the variation of the elastic constants C_{11}, C_{12} and C_{44} with respect to applied pressure. Within the pressure range considered, there is a linear dependence in all the constants with respect to pressure. The C_{11}, which is associated with the elasticity in the longitudinal distortion, increases rapidly with pressure. However, C_{12} and C_{44} are less sensitive to change in pressure. Since all the elastic constants are determined directly from the average bond strength features, C_{11} increases due to decrease in bond length and increase in charge density as pressure increases. But, the enhancement of the bond strength has little effect on the shear deformation resistance due to lesser changes in C_{44} when the applied pressure is enhanced.[34]

4. Conclusions

Employing first-principles calculations based on density functional theory within the GGA and PAW, we have extensively studied the structural, electronic, elastic and mechanical properties of ZrNiPb half-Heusler alloy. The calculated lattice constant and bulk modulus are in good agreement with the available experimental and theoretical data. We found and confirmed that ZrNiPb is an indirect bandgap semiconductor alloy with a narrow-bandgap of 0.375 eV. The inter-atomic distances for Zr–Pb and Pb–Ni was reported as 3.124 and 2.705 Å at zero pressure. Also, we predicted that under applied pressure, Pb–Ni bond is more sensitive to pressure than Zr–Pb bond and the degree of covalence in ZrNiPb half-Heusler alloy is bond length-dependent. Between 0 and 30 GPa, we reported that there is no possibility for semiconductor-metal transition in ZrNiPb half-Heusler alloy. From our calculation of the DOS and PDOS, it was established that there is a strong hybridization effect which could lead to bond and anti-bonding orbital separation in ZrNiPb half-Heusler alloy and could contribute to its stability. We also found that ZrNiPb is structurally stable and there is no possibility of phase transformation in the pressure range considered in this work. We also established that under pressure, ZrNiPb is a favorable thermoelectric material due to the low value of its G/B ratio. At zero pressure, we confirmed that ZrNiPb is a brittle material with B/G ratio of 1.51.

Acknowledgments

The authors are grateful to the Marie Curie Library of the Abdus Salam International Centre for Theoretical Physics (ICTP) for permission to use the eJDS facility for reference searching. Two of us, BIA and Dr. Abu Yaya, acknowledge the Centre for High Performance Computing (CHPC) South Africa for computer time on their clusters.

References

1. F. Yan *et al.*, *Nat. Commun.* **6**, 7308 (2015), doi:10.1038/ncomms8308.
2. P. Qiu *et al.*, *Appl. Phys. Lett.* **96**, 152105 (2010), http://dx.doi.org/10.1063/1.3396981.
3. P. Qiu *et al.*, *J. Appl. Phys.* **106**, 103703 (2009), doi:10.1063/1.3238363.
4. G. Ding, G. Gao and K. Yao, *J. Appl. Phys.* **119**, 025105 (2016), http://dx.doi.org/10.1063/1.4939887.
5. S. Sharma and S. Pandey, *J. Phys.: Condens. Matter* **26**, 215501 (2014), doi:doi.org/10.1088/0953-8984/26/21/215501.
6. J. Mena *et al.*, *J. Alloys Compd.* **650**, 728 (2015), https://doi.org/10.1016/j.jallcom.2015.07.193.
7. R. Gautier *et al.*, *Nat. Chem.* **7**, 308 (2015), doi:10.1038/nchem.2207.
8. G. Wang and D. Wang, *J. Alloys Compd.* **682**, 375 (2016), doi:10.1016/j.jallcom.2016.05.013.
9. G. Rogl *et al.*, *Acta Mater.* **107**, 178 (2016), doi:10.1016/j.actamat.2016.01.031.
10. Y. Kawaharada *et al.*, *J. Alloys Compd.* **381**, 9 (2004), https://doi.org/10.1016/j.jallcom.2004.03.103.
11. M. Verges *et al.*, *Sci. Adv. Mater.* **3**, 659 (2011), https://doi.org/10.1166/sam.2011.1197.
12. M. Hichour *et al.*, *J. Phys. Chem. Solids* **73**, 975 (2012), https://doi.org/10.1016/j.jpcs.2012.03.014.
13. B. Kong *et al.*, *J. Alloys Compd.* **509**, 2611 (2011), https://doi.org/10.1016/j.jallcom.2010.11.119.
14. D. Wang and G. Wang, *Phys. Lett. A* **381**, 801 (2017), http://dx.doi.org/10.1016/j.physleta.2016.10.039.
15. A. Bouhemadou and R. Khenata, *J. Appl. Phys.* **102**, 043528 (2007), http://dx.doi.org/10.1063/1.2773634.
16. J. Perdew and A. Zunger, *Phys. Rev. B* **23**, 5048 (1981), https://doi.org/10.1103/PhysRevB.23.5048.
17. P. Giannozzi *et al.*, *J. Phys.: Condens. Matter* **21**, 395502 (2009), https://doi.org/10.1088/0953-8984/21/39/395502.
18. http://qe-forge.org/gf/project/pslibrary.

19. C. Broyden, *J. Inst. Math. Appl.* **6**, 76 (1970).
20. H. Monkhorst and J. Pack, *Phys. Rev. B* **13**, 5188 (1976), https://doi.org/10.1103/PhysRevB.13.5188.
21. M. J. Mehl, *Phys. Rev. B* **47**, 2493 (1993), https://doi.org/10.1103/PhysRevB.47.2493.
22. S. Q. Wang and H. Q. Ye, *J. Phys.: Condens. Matter.* **15**, 5307 (2003), https://doi.org/10.1088/0953-8984/15/30/312.
23. B. I. Adetunji *et al.*, *Solid State Commun.* **178**, 46 (2014), http://dx.doi.org/10.1016/j.ssc.2013.10.008.
24. F. Murnaghan, *Proc. Natl. Acad. Sci. USA* **30**, 244 (1944).
25. S. Guo, *RSC Adv.* **6**, 47953 (2016), doi:10.1039/C6RA08461C.
26. S. Ogut and K. M. Rabe, *Phys. Rev. B* **51**, 10443 (1995), https://doi.org/10.1103/PhysRevB.51.10443.
27. P. Vajeeston *et al.*, *Phys. Rev. B* **63**, 045115 (2001), https://doi.org/10.1103/PhysRevB.63.045115.
28. P. Mao *et al.*, *J. Appl. Phys.* **117**, 115903 (2015), http://dx.doi.org/10.1063/1.4915339.
29. M. M. Wu *et al.*, *J. Alloys Compd.* **506**, 412 (2010), doi:10.1016/j.jallcom.2010.07.018.
30. A. Hong *et al.*, *J. Mater. Chem. C* **4**, 3281 (2016), doi:10.1039/C6TC00461J.
31. J. Wang, Y. Zhou and Z. Lin, *Acta Mater.* **55**, 6019 (2007), https://doi.org/10.1016/j.actamat.2007.07.010.
32. S. F. Pugh, *Philos. Mag.* **45**, 823 (1954), http://dx.doi.org/10.1080/14786440808520496.
33. T. Seddik *et al.*, *Appl. Phys. A* **106**, 645 (2012), doi:10.1007/s00339-011-6643-2.
34. F. Gu *et al.*, *Phys. Scr.* **89**, 105703 (2014), doi:10.1088/0031-8949/89/10/105703.